DOI: 10.1002/chem.200903370

Growth of Shape- and Size-Selective Zinc Oxide Nanorods by a Microwave-Assisted Chemical Bath Deposition Method: Effect on Photocatalysis Properties

Vaishali R. Shinde,*[a] Tanaji P. Gujar,[b] Takeshi Noda,[a] Daisuke Fujita,[a] Ajayan Vinu,[b] Mathieu Grandcolas,[a] and Jinhua Ye[c]

Abstract: Herein, we demonstrate the shape- and size-selective growth of ZnO nanostructures on indium tin oxide-coated glass substrates by using a microwave-assisted chemical bath deposition method. By systematically controlling the deposition parameters, it is possible to produce shape- and size-selective nanostructures with high alignment and uniformity. Specifically, the pH of the bath can be used to control the shape of rods from bundled structures to tapered and flat tips. Furthermore, the deposition temperature can be used to control the size of the ZnO array from 770 to 125 nm. The prepared rods were active catalysts in the degradation of methylene blue under UV radiation, and exhibited size-dependent activity.

Keywords: crystal engineering · crystal growth · nanostructures · photocatalysis · zinc

Introduction

Zinc oxide (ZnO), a semiconductor with a direct bandgap of 3.37 eV and a large exciton binding energy of 60 meV, possesses unique electrical, optoelectronic, and luminescent properties.[1–7] Because of these attractive properties, nanostructured ZnO, including particles, rods, wires, belts, tubes, and disks, have many important practical applications in catalysis, photoluminescence, and functional devices (e.g., solar cells, resonators, field-effect transistors, and gas sensors).[8–14] It is reasonable to state that ZnO, in the form of one-dimensional (1D) nanostructures, is one of the most studied and the most important 1D nanomaterials after carbon nanotubes and silicon nanowires in today's research. Because of access of various ZnO nanostructures, many possible nanostructures of ZnO are already being explored. Accordingly, future research into ZnO nanostructures has a lot of scope and should be concentrated on the study of the fundamentals of growth kinetics, structural control, morphology, dimensionality, and, most importantly, low-cost and large-scale production, along with the possibility of patterned growth and self-organization.[15] Of the abovementioned factors, we are concerned with the ability to control both the shape and size of nanocrystals over large areas by using low-cost chemical methods. The control of the shape and size of nanocrystals is crucial for tuning their optical and electronic properties and the overall functionality for their proposed application because the size and shape of inorganic materials are important factors in determining their electrical, optical, and other properties.[16–18]

To control the shape and size of ZnO, it becomes necessary to examine the crystal symmetry and growth habit of ZnO, which has been discussed in several reports.[19,20] It is known that due to the presence of oxygen vacancies and/or zinc interstitial atoms, ZnO is an intrinsic n-type semiconductor.[21] The thermodynamic stable crystal structure of ZnO is wurtzite, which has the space group *P*6*mc* (No. 186), and can be described as an hcp array of Zn atoms at (1/3, 2/3, 0) and (2/3, 1/3, 1/2) in which oxygen atoms occupy half

[a] Dr. V. R. Shinde, Dr. T. Noda, Prof. D. Fujita, Dr. M. Grandcolas
International Center for Young Scientists
National Institute for Materials Science (NIMS)
Sengen 1-2-1, Tsukuba, Ibaraki 305-0047 (Japan)
Fax: (+81) 29-859-2200
E-mail: shinde_vr2003@yahoo.com

[b] Dr. T. P. Gujar, Dr. A. Vinu
International Center for Materials Nanoarchitectonics
National Institute for Materials Science (NIMS)
1-1 Namiki, Tsukuba, Ibaraki 305-0044 (Japan)

[c] Dr. J. Ye
International Center for Materials Nanoarchitectonics
Photocatalytic Materials Center
National Institute for Materials Science (NIMS)
Sengen 1-2-1, Tsukuba, Ibaraki 305-0047 (Japan)

of the tetrahedrally coordinated sites at (1/3, 2/3, 3/8) and (2/3, 1/3, 7/8). This results in a noncentrosymmetric crystal comprised of alternating planes of tetrahedrally coordinated O^{2-} and Zn^{2+} ions stacked alternately along the *c* axis. The atomic arrangements on the low-index planes of the hexagonal prism on ZnO, $\{10\bar{1}0\}$ and $\{11\bar{2}0\}$, are stoichiometric with equal numbers of exposed Zn^{2+} or O^{2-} ions, whereas the basal planes, (0001) and $(000\bar{1})$, and the pyramidal planes, $\{10\bar{1}1\}$, are strongly polar and consist of sheets of Zn^{2+} or O^{2-}. The polar zinc-terminated surface is usually designated as (0001) and the polar oxygen-terminated surface as $(000\bar{1})$.[20,22] Generally, the positively Zn^{2+}-terminated (0001) and negatively O^{2-}-terminated $(000\bar{1})$ polar surfaces have high surface energies, and the growth of the crystal will be preferentially along the *c* axis. Thus, depending on the structural anisotropy and surface electric polarity of ZnO, the growth rate is highest for [0001], decreases for $[\bar{1}01\bar{1}]$, $[\bar{1}010]$, $[\bar{1}011]$, and is lowest for $[000\bar{1}]$ under normal conditions.[22,23] Consequently, by controlling the thermodynamics and kinetics of nucleation and growth rates, specific ZnO facets can be passivated and by adjusting the growth velocity order of the ZnO facets, the shape and size can be controlled, which is possible by controlling the experimental parameters.[24,25] This control can be comparatively easily implemented in solution-based methods. Low-temperature-solution chemical processes, such as precipitation, hydrolysis, and the hydrothermal process, are widely used in the synthesis of a variety of ZnO nanostructures.[26] These methods are economical and suitable for large-scale production. ZnO nanorods (NRs) have been successfully synthesized by using the hydrothermal process. However, the entire reaction generally needs a longer time, and the use of catalysts or templates introduces impurities into the desired product. The microwave process provides fast and homogeneous heating, which leads to more rapid and simultaneous nucleation, high yields, high purity, and lower cost.

Herein, shape- and size-selective ZnO NRs have been synthesized by using a microwave-assisted chemical bath deposition (MWCBD) method. We have controlled the growth rate to control the shape and size of the ZnO product by changing the solution pH and the growth temperature. In particular, the growth rate of ZnO has been controlled in such a way that the shape of the ZnO NRs changes from tapered to flat, and the size continued to reduce as a consequence of changes in the pH and temperature of the solution.

Results and Discussion

The MWCBD is a method of controlled precipitation under microwave irradiation, and is based on the formation of a solid phase upon the transformation of a supersaturated solution to the saturated state. Two distinct steps, nucleation and subsequent particle growth, are involved in this process. During nucleation, clusters of metal precursor molecules probably undergo rapid decomposition. Subsequently, the film grows to a certain thickness on the substrate surface through the coalescence of particles.[27] The preparation of ZnO NRs in this work has been achieved by heating a supersaturated aqueous $Zn(NO_3)_2$ solution prepared by the addition of aqueous NH_3. The indium tin oxide (ITO) substrate is immersed in the solution during this process.

There are several possible soluble and insoluble Zn^{2+} species with ligands such as OH^-, H_2O, NO_3^-, and NH_3 in the reaction bath. For a solution containing $Zn(NO_3)_2$ salt with a concentration of around 0.01 M, Zn is soluble as hydrated Zn^{2+} at a pH value of 7 [Eq. (1)].

$$m\mathrm{Zn(NO_3)_2} + mp\mathrm{H_2O} \rightarrow m[\mathrm{Zn(H_2O)}_p]^{2+} + 2m(\mathrm{NO_3})^- \ (\mathrm{pH} \approx 7) \quad (1)$$

A soluble $[Zn(NH_3)_q]^{2+}$ ($q = 1$–4) complex is produced at pH values higher than 10, whereas in the intermediate pH range of between 7 and 10, insoluble $Zn_m(OH)_{2m}$ is formed because the pH of the solution affects the hydrolysis equilibrium of NH_3. However, insoluble $Zn_m(OH)_{2m}$ is not the sole product obtained when aqueous NH_3 is added to aqueous $Zn(NO_3)_2$ in the intermediate pH region. During the precipitation process, hydrated zinc ion complexes ($m[Zn(H_2O)_2]^{2+}$) are transformed into zinc hydroxide ($[Zn_m(OH)_{2m}]$) through stepwise replacement of water molecules by hydroxide groups; this process is referred to as "olation", as depicted by Equation (2).

$$\begin{aligned} m[\mathrm{Zn(H_2O)}_p]^{2+} + r(\mathrm{OH})^- &\leftrightarrow [\mathrm{Zn}_m(\mathrm{OH})_r(\mathrm{H_2O})_{mp-r}]^{(2m-r)+} \ (\mathrm{pH} < 9) \\ \text{and} \quad &\leftrightarrow \mathrm{Zn}_m(\mathrm{OH})_{2m(\mathrm{s})} \text{ or } m\mathrm{Zn(OH)_2} \ (\mathrm{pH} \approx 9) \end{aligned} \quad (2)$$

Upon further addition of aqueous NH_3, the white $Zn(OH)_2$ precipitate is dissolved and a clear solution is obtained at a pH value close to 10. The addition of aqueous NH_3 reduces the $Zn(OH)_2$ precipitate to produce complex ions $[Zn(NH_3)_q]^{2+}$ ($q = 1$–4), in which $q = 4$ is the most stable coordination number for Zn. The formation of complex ions prevents spontaneous precipitation and leads to formation of a supersaturated state, as shown in Equation (3).

$$\begin{aligned} &\mathrm{Zn}_m(\mathrm{OH})_{2m}/[m\mathrm{Zn(OH)_2}] + q\mathrm{NH_4}^+ + q(\mathrm{OH})^- \\ &\leftrightarrow \mathrm{Zn}_m(\mathrm{NH_3})_q{}^{2m+} + q\mathrm{H_2O} + 2m(\mathrm{OH})^- \ (\mathrm{pH} > 10) \end{aligned} \quad (3)$$

An equilibrium state is established in the reaction bath after the solution becomes supersaturated. Upon heating this solution, the release of NH_3 from the reaction system disturbs the equilibrium and the pH of the reaction bath consequently decreases. When this solution, along with the immersed substrates, is heated, the complex $Zn_m(NH_3)_q{}^{2m+}$ is then decomposed under microwave irradiation to form the ZnO product by releasing H_2O and NH_3, and precipitation occurs by heterogeneous growth on the substrate as shown in Equation (4).

$$[Zn_m(NH_3)_q]^{2m+} + 2m(OH)^- \rightarrow mZnO + mH_2O + qNH_{3(g)} \quad (4)$$

The crystallographic structure of the ZnO films on ITO substrates obtained by heating supersaturated alkaline zinc nitrate solution at different pH values (10.0, 10.5, 11.0, 11.5, 12.0) has been studied by XRD. The concentration of Zn^{2+} was fixed at 0.01 M and the temperature of deposition was 90 °C. Figure 1 shows the XRD patterns of the sample prepared at 90 °C at different pH values. All the patterns show the formation of the wurtzite ZnO structure with a dominant peak at ≈34.4° (JCPDS No. 36-1451), which corresponds to a (002) reflection and indicates the polycrystalline nature of the films with a preferred *c*-axis orientation. The intensity of the (002) peak was found to increase as the pH was increased. The increase in intensity of the (002) peak indicates that the increase in the pH of the reaction bath improves the crystalline nature of deposited ZnO NR arrays.

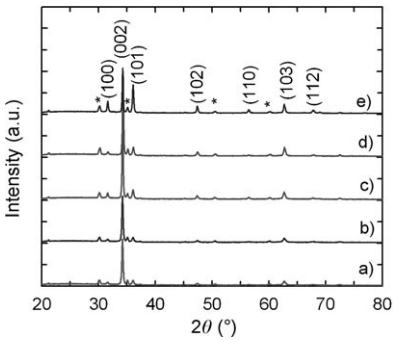

Figure 1. XRD patterns of ZnO films prepared at pH values of a) 10.0, b) 10.5, c) 11.0, d) 11.5, and e) 12.0 at $T = 90$ °C. *: ITO substrate peaks.

Further SEM studies proved the pH-induced shape and size variation, as shown in Figure 2. For example, at pH 10.0 agglomerated ZnO NRs with some walls connected to give hexagonal bundled structures were obtained, (Figure 2a). Along with the bundled microrods, individual microrods are also observed. On increasing the pH to 10.5, a larger amount of ZnO microrods with relatively smaller diameters were grown (Figure 2b). Interestingly, the shape of the ZnO NRs changed from hexagonal to tapered as the pH value was increased, which can be seen from the SEM image. This shape transformation can be explained in terms of the differences in the growth rates of various crystal faces. In general, the crystal plane with the highest growth rate disappears quickly, thus making the relative growth rate crucial for determination of morphology of crystal. At low pH (i.e., 10), the growth rate of the crystal planes is likely to be random or, more specifically, the growth rate at low pH is higher along the $(10\bar{1}0)$ or $(01\bar{1}0)$ crystal planes that form the sides of the hexagonal rods. As a consequence, the surface energy of these planes becomes higher and they tend to either grow in the same direction or reduce the surface

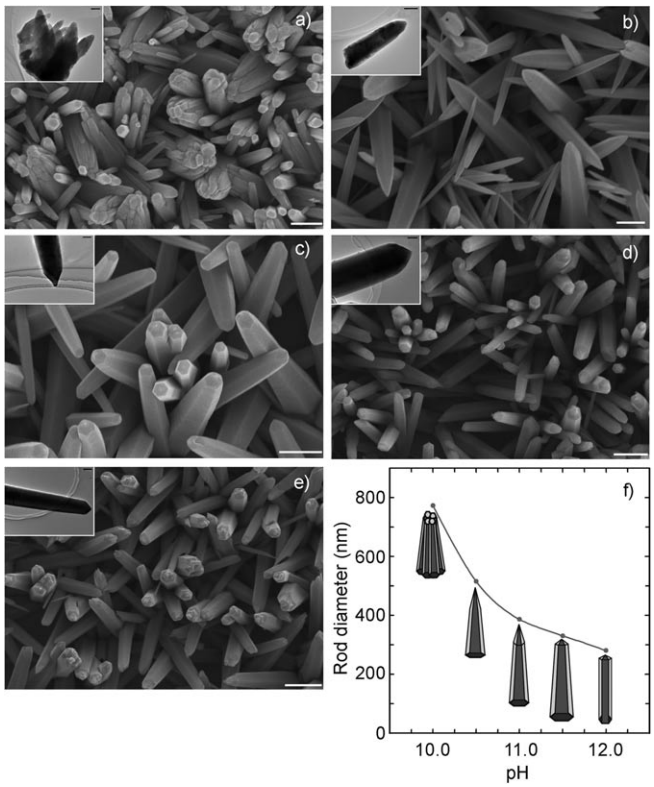

Figure 2. SEM images of ZnO films prepared at pH values of a) 10.0, b) 10.5, c) 11.0, d) 11.5, and e) 12.0 at $T = 90$ °C; scale bars = 500 nm. Insets of a)–e) show the TEM images of the tip of an individual rod; inset scale bars = 200 nm (a, b), 100 nm (c, d, e). f) Dependence of rod shape and size on the pH.

energy by capturing smaller particles to reduce their surface energy.[28] Thus at pH 10, the growth resulted in the hexagonal bundled structure of ZnO (Figure 2a). On the other hand, as the pH is increased further, the kinetics of nucleation and growth are changed and in turn the morphology is changed to tapered single rods. In this case, the growth rate of the (0001) crystal face of the wurtzite structure of ZnO is highest and thus during the growth process this face easily disappears, resulting in a pointed shape at the end of the *c* axis. Meanwhile, the opposite face of the *c* axis, that is, $(000\bar{1})$, which is attached to the substrate, gives a flat shape due to the slowest growth rate (Figure 2b).[29] For further increases in the pH value of the reaction bath, a decrease in size and a flattening of the tip is observed (Figure 2c to e). The inset of each SEM image shows TEM images of tip of the ZnO rods obtained at different pH values, and clearly confirms the change in the tip shape. There are two possible mechanisms for the flattened tip and decreased size of the ZnO rods at higher pH values. The decrease in rod size can be explained on the basis of the classical theory of nucleation, which demonstrates that an increase in the pH of a supersaturated solution causes an increase in the nucleation rate, which is a consequence of a decrease in nucleation activation energy. Thus, the increase in supersaturation with increasing pH causes the bursting of a larger number of nuclei

at higher pH values and consequently ZnO crystals with smaller size are formed.[30] At the same time, the growth rate of the (0001) plane is probably restricted because of the fast nucleation and slow growth rate that results in the flat-tipped ZnO NRs. Another scenario could be the competition between growth and erosion.[31] As explained above, the hexagonal wurtzite ZnO crystal with a dipole moment in the direction of the *c* axis is a typical polar crystal, so the (0001) crystal plane is metastable and the non-polar side planes are relatively more stable. The polar top plane attracts OH^- ions from the solution, and causes erosion of the tip of the rods in solution. At low pH values, the OH^- concentration in solution is sufficient for the growth of NRs, however, above a certain pH value the total amount of OH^- becomes an excess and cannot be totally consumed during growth. The remaining OH^- in solution causes the erosion of the grown rods. With the increase in pH, the relative erosion process becomes intensive. However, during growth from the supersaturated solution, the growth rate will be faster than the rate of erosion. Thus due to the competition between growth and erosion, the tops of the ZnO NRs become flat in shape and rod size is decreased. Additionally, due to the differences in growth rate and active erosion, the size distribution of the ZnO rods continues to improve. Thus by changing the pH of the solution, the shape and size can be varied significantly and good size distribution can be achieved. Figure 2f shows the variation in average diameter measured at the centre of the rods; the diameter varies from $\approx$770 to 300 nm as the pH of the reaction bath increases, and the corresponding shapes of the ZnO NRs are shown below the graph. Figure 2 clearly illustrates the pH-induced shape and size variation from bundled to tapered and flat tip ZnO NR arrays on the substrate. Thus, we may conclude that an increase in the pH of the solution induces changes in the kinetics of nucleation and growth so that the growth rates along lateral planes and the *c* axis are modified, accompanied by erosion of the rods, which results in a variation of shape and size of the ZnO rods on the substrates.

Figure 3 shows SEM images of ZnO NRs on the substrate obtained at different temperatures (100, 110, and 120 °C) and pH values (10.0 and 12.0). For each deposition temperature, a change in the shape and size is observed, similar to the effect of pH observed above and arising from similar mechanisms. Furthermore, it can be seen from the SEM images that the diameter of the rods decreases with increasing temperature at a constant pH value. In general, two opposing trends occur at higher temperatures: at higher deposition temperatures, the rate of ionic diffusion onto a substrate and interdiffusion between separate crystals increases and the influence of the activation energy decreases, leading to larger crystals. The opposing factor is the increased nucleation rate at higher temperatures, which results in higher crystallinity and a decrease in the diameter of the NRs due to the solubility of ZnO with temperature. The first factor apparently dominates at lower temperatures, whereas the second dominates at higher temperatures. Therefore, the size of ZnO rods shows a decreasing trend with increasing

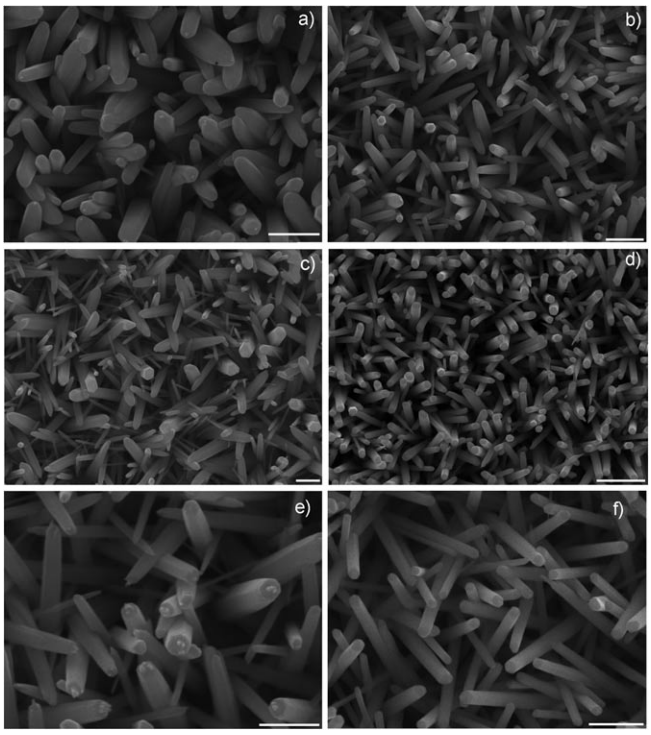

Figure 3. SEM images of ZnO at $T = 100$ (a, b), 110 (c, d), and 120 °C (e, f) at pH values of 10 (a, c, e) and 12 (b, d, f); scale bars = 500 nm.

temperature.[30,32] Figure 4 shows the variation in rod diameter with pH value at 100, 110, and 120 °C. For each temperature, the diameter range is higher at low pH values and lower at higher pH values, which gives rise to uniformly sized ZnO NRs. The smallest ZnO NRs (125 nm) with the best homogeneity were obtained at pH 12.0 and a temperature of 120 °C. Figure 5 shows HRTEM and selected area electron diffraction (SAED) images of ZnO NRs obtained at 120 °C and pH 12.0. The high-resolution image suggests that the growth of ZnO is along the *c* axis, which corresponds to the [0001] direction. The SAED pattern acquired from same sample shows that the growth direction of the rods is along the *c* axis. Moreover, the HRTEM image clearly shows an absence of stacking defects in the crystalline structure, which suggests that the crystals of individual rods are of good quality.

ZnO is a very promising photocatalyst, especially for the mineralization of organic pollutants dissolved in solution, and results in efficient photodegradation of organic compounds under UV irradiation.[33–35] However, it is worth noting that when commercial ZnO or nanostructured ZnO powder is used for removing organic compounds from aqueous solution, the separation of the conventional ZnO powder photocatalyst from the reacting aqueous suspension becomes a major problem for reuse in photocatalytic processes.[36] Therefore, 1D ZnO films, especially well-aligned ZnO nanostructures on the substrates, would be more stable and convenient for reuse; thus it is possible to overcome the disadvantage of removal of ZnO powder and to extend the

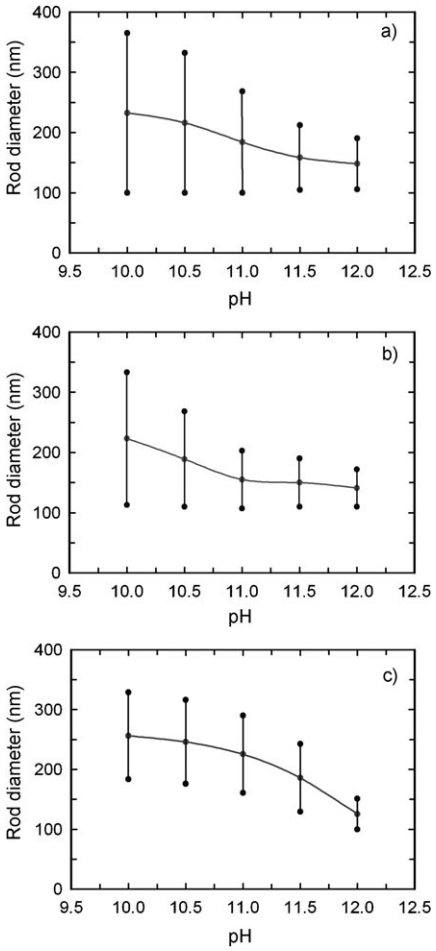

Figure 4. Dependence of ZnO rod size on pH at a) 100, b) 110, and c) 120 °C.

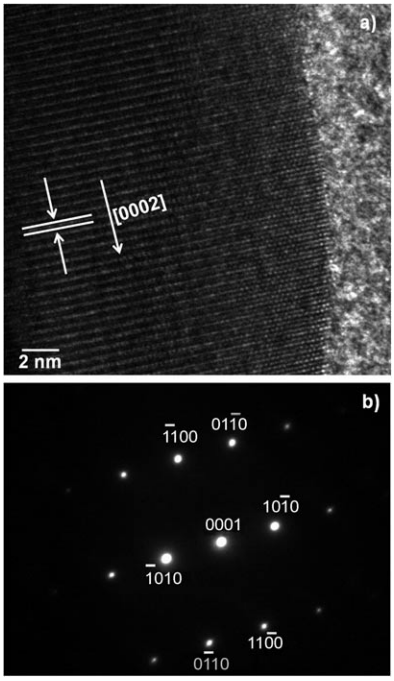

Figure 5. a) HRTEM and b) SAED images of ZnO NRs grown at 120 °C and pH 12.

industrial applications of ZnO in environmental treatments. Herein we have studied the photocatalysis of two different sizes of ZnO NRs (synthesized at pH 10 and 12 at $T=$ 120 °C). The absorption spectra of methylene blue (MB) after undergoing photocatalytic degradation by ZnO NRs of different sizes are shown in Figure 6a and b. The optical absorption spectrum of MB features three bands centered at $\lambda=664$, 292 nm, of which the $\lambda=664$ nm absorption band arises from the chromophore in MB and the two bands in the ultraviolet region originate from benzene rings. The band at $\lambda=664$ nm was selected to monitor the change in MB concentration over time. These results demonstrate that the conjugated structure of MB was broken up and transformed into small aromatic intermediates. As the irradiation time increased, the absorption intensity of the bands at $\lambda=$ 664 and 292 nm decreased smoothly, which suggests further decomposition of the aromatic intermediates. Additionally, after irradiation for 2 h, larger ZnO NRs (pH 10, $T=$ 120 °C) photodegraded 85 % of MB whereas smaller ZnO NRs (pH 12, $T=120$ °C) degraded 92 % of MB under the

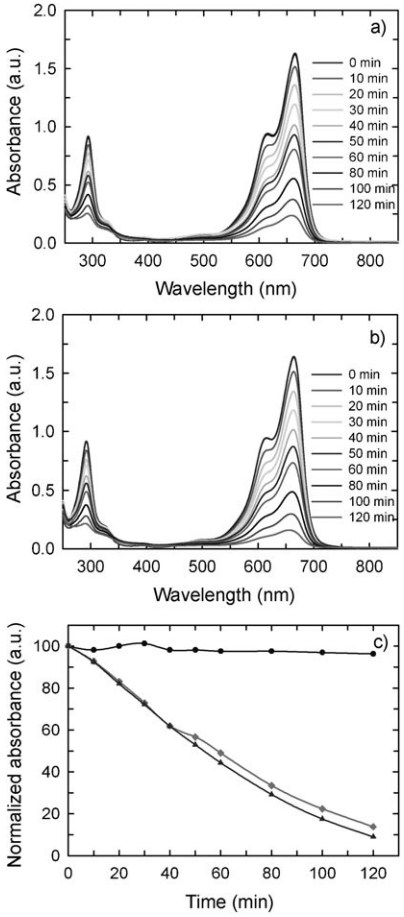

Figure 6. UV/Vis spectra for the photocatalytic degradation of MB in the presence of ZnO NRs synthesized at 120 °C and a) pH 10 or b) pH 12. c) Profile of percentage decomposition vs. time for ZnO NRs; ●: dye, ◆: ZnO at pH 10, ▲: ZnO at pH 12.

same experimental conditions (Figure 6b). Figure 6c shows the normalized degradation of MB in presence of ZnO NRs of different sizes and clearly indicates that the smaller ZnO NRs (pH 12, $T=120\,°C$) show an enhancement in photocatalytic activity that is believed to be related to the surface area. As well as the surface area for photocatalytic activity, the facets and orientation of ZnO are also important factors. Polar *c* surfaces have higher photocatalytic activity for the decomposition of MB than nonpolar planes.

Conclusion

In summary, wurtzite ZnO NR arrays were synthesized by using a simple and fast MWCBD at different temperatures, with the pH controlled by using NH_3. We have successfully demonstrated that the size and shape evolution of ZnO NRs array by soft-solution chemistry method and studied their shape evolution mechanism by applying crystallographic concepts. The size, shape, diameter, and effective aspect ratio of the NRs are readily tuned by modifying the reaction bath pH and deposition temperature. The morphology (bundled, tapered tip, and flat tip) and size of the ZnO NRs can be controlled by changing the pH and temperature of the reaction bath. In particular, an increase in the pH of the solution promotes the nucleation rate, resulting in a decrease of size of the rods and modification of the growth rates along different planes to give varying shapes and sizes of rods. The high crystallinity and surface area of ZnO NRs show excellent photocatalytic performance due to the high chemical activity of the (002)-oriented NRs and the activity is size dependent. Our results demonstrate that it is feasible to use reactive and stable ZnO NR arrays for repeated application in photocatalysis. In addition, the present study supports the fundamental study of ZnO and a method of improving application performance with reactive, stable, and oriented ZnO and other metal oxides, which have promising applications as photocatalysts, solar cells, and optoelectronic devices.

Experimental Section

An aqueous solution of $Zn(NO_3)_2$ (10 mM; Aldrich Chemicals) was prepared and aqueous NH_3 (28%; Aldrich Chemicals) was added under constant stirring. A white precipitate was initially observed, which subsequently dissolved back in solution upon further addition of aqueous NH_3. The pH of the solution at this stage was ≈ 10. The ITO-coated glass substrates were used for all depositions. The substrate cleaning step is crucial for the growth of materials and the substrates were initially cleaned with detergent and degreased in an ultrasonic cleaner for 30 min. The detergent was replaced with acetone and the substrate was again degreased in an ultrasonic cleaner for 30 min. Finally the acetone was replaced with isopropyl alcohol and the substrates were kept immersed in it. Before use, the substrate was cleaned with distilled water and dried under an argon flow. A pre-cleaned ITO substrate coated with a thin layer of ZnO was immersed vertically in the $Zn(NO_3)_2$ solution, which was heated by using microwave irradiation (Milestone multisynthetic labstation) to a specific temperature for 1 h to give the direct growth of NR arrays on the ITO substrate. The pH of the bath was varied from 10.0 to 12.0 by addition of different amounts of aqueous ammonia. The temperature was varied from 90 to 120 °C. The substrate with the deposited ZnO nanostructures was then removed from the bath, washed with deionized water, dried under air, and used for further characterization. The phase identification of the sample deposited on the ITO substrate was carried out by using XRD patterns that were collected by using a Rigaku diffractometer with $Cu_{K\alpha 1}$ radiation ($\lambda=1.5406$ Å), operated at 40 kV and 250 mA. The diffractograms were recorded in the 2θ range of 20 to 80° with a 2θ step size of 0.02°. The morphology and size of the ZnO nanostructures were characterized by FESEM by using a JSM-7100F instrument with an accelerating voltage of 15.0 kV. For further insight into the microstructure of the NRs, TEM and HRTEM images were recorded by using a Hitachi H-800 instrument at 200 kV or a JEOL-2010 instrument at 200 kV equipped with an X-ray EDS device. For the evaluation of catalyst activity, the ZnO NR film (2×2 cm) was suspended in an aqueous solution of MB (1×10^{-4} M, 100 mL, pH 7; Wako) in a Pyrex reactor. A Xe lamp (300 W) equipped with a cut-off filter (L42) and a water filter was used as the light source. The average intensity of the incident light was approximately 53.1 mW cm^{-2}. At given time intervals, approximately 3 mL of the reaction suspension was sampled. The absorption spectrum of the filtrate was measured by using a Shimadzu UV-2500PC UV/Vis spectrometer. The concentration of MB was determined by monitoring the changes in the absorbance maximized at approximately $\lambda=650$ nm.

Acknowledgements

V.R.S. acknowledges the National Institute for Materials Science for International Center for Young scientist (ICYS) Fellowship. This work is also supported by the Japan Society for the Promotion of Science through a Grant-in-Aid (Kakenhi for Young Scientist B) for Scientific Research of Japan (21760055).

[1] X. D. Wang, J. H. Song, J. Liu, Z. L. Wang, *Science* **2007**, *316*, 102–105.
[2] G. Begum, S. V. Manorama, S. Singh, R. K. Rana, *Chem. Eur. J.* **2008**, *14*, 6421–6427.
[3] M. H. Huang, S. Mao, H. Feick, H. Yan, Y. Wu, H. Kind, E. Weber, R. Russo, P. Yang, *Science* **2001**, *292*, 1897–1899.
[4] L. Liao, H. B. Lu, J. C. Li, H. He, D. F. Wang, D. J. Fu, C. Liu, *J. Phys. Chem. C* **2007**, *111*, 1900–1903.
[5] H. Saal, M. Binnewies, M. Schrader, A. Bcrger, K. D. Becker, V. A. Tikhomirov, K. Jug, *Chem. Eur. J.* **2009**, *15*, 6408–6414.
[6] C. M. Lieber, Z. L. Wang, *MRS Bull.* **2007**, *32*, 99–108.
[7] F. Patolsky, C. M. Lieber, *Mater. Today* **2005**, *8*, 20–28.
[8] M. Monge, M. L. Kahn, A. Maisonnat, B. Chaudret, *Angew. Chem.* **2003**, *115*, 5479–5482; *Angew. Chem. Int. Ed.* **2003**, *42*, 5321–5324.
[9] Z. W. Pan, Z. R. Dai, Z. L. Wang, *Science* **2001**, *291*, 1947–1949.
[10] Q. Zhang, T. P. Chou, B. Russo, S. A. Jenekhe, G. Cao, *Angew. Chem.* **2008**, *120*, 2436–2440; *Angew. Chem. Int. Ed.* **2008**, *47*, 2402–2406.
[11] V. R. Shinde, T. P. Gujar, C. D. Lokhande, R. S. Mane, S. H. Han, *Mater. Sci. Eng. B* **2007**, *137*, 119–125.
[12] V. R. Shinde, T. P. Gujar, C. D. Lokhande, *Sens. Actuators B* **2007**, *120*, 551–559.
[13] J. Zhou, N. Xu, Z. L. Wang, *Adv. Mater.* **2006**, *18*, 2432–2435.
[14] S. M. Al-Hilli, R. T. Al-Mofarji, M. Willander, *Appl. Phys. Lett.* **2006**, *89*, 173119.
[15] Z. L. Wang, *ACS Nano* **2008**, *2*, 1987–1992.
[16] Y. W. Chen, Q. Qiao, Y. C. Liu, G. L. Yang, *J. Phys. Chem. C* **2009**, *113*, 7497–7502.
[17] L. Vayssieres, A. Hagfeldt, S. E. Lindquist, *Pure Appl. Chem.* **2000**, *72*, 47–52.
[18] S. H. Jung, E. Oh, K. H. Lee, Y. Yang, C. G. Park, W. Park, S. H. Jeong, *Cryst. Growth Des.* **2008**, *8*, 265–269.
[19] M. S. Mo, D. Wang, X. Du, J. Ma, X. Qian, D. Chen, Y. Qian, *Cryst. Growth Des.* **2009**, *9*, 797–802.

[20] C. Woll, *Prog. Surf. Sci.* **2007**, *82*, 55–120.
[21] V. R. Shinde, C. D. Lokhande, R. S. Mane, S. H. Han, *Appl. Surf. Sci.* **2005**, *245*, 407–413.
[22] L. Xu, Y. L. Hu, C. Pelligra, C. H. Chen, L. Jin, H. Huang, S. Sithambaram, M. Aindow, R. Joesten, S. L. Suib, *Chem. Mater.* **2009**, *21*, 2875–2885.
[23] K. X. Yao, H. C. Zeng, *J. Phys. Chem. B* **2006**, *110*, 14736–14743.
[24] L. Vayssieres, M. Graetzel, *Angew. Chem.* **2004**, *116*, 3752–3756; *Angew. Chem. Int. Ed.* **2004**, *43*, 3666–3670.
[25] J. Zhang, H. Liu, Z. Wang, N. Ming, Z. Li, A. S. Biris, *Adv. Funct. Mater.* **2007**, *17*, 3897–3905.
[26] E. DelaRosa, S. Seplveda-Guzman, B. Reeja-Jayan, A. Torres, P. Salas, N. Elizondo, M. J. Yacaman, *J. Phys. Chem. C* **2007**, *111*, 8489–8495.
[27] V. R. Shinde, H. S. Shim, T. P. Gujar, H. J. Kim, W. B. Kim, *Adv. Mater.* **2008**, *20*, 1008–1012.
[28] B. L. Cushing, V. L. Kolesnichenko, C. J. O'Connor, *Chem. Rev.* **2004**, *104*, 3893–3946.
[29] Z. Dai, K. Liu, Y. Tang, X. Yang, J. Bao, J. Shen, *J. Mater. Chem.* **2008**, *18*, 1919–1926.
[30] D. Chu, T. Hamada, K. Kato, Y. Masuda, *Phys. Status Solidi A* **2009**, *206*, 718–723.
[31] M. Willander, L. L. Yang, A. Wadeasa, S. U. Ali, M. H. Asif, Q. X. Zhao, O. Nur, *J. Mater. Chem.* **2009**, *19*, 1006–1018.
[32] J. Zhao, Z. G. Jin, X. X. Liu, Z. F. Liu, *J. Eur. Ceram. Soc.* **2006**, *26*, 3745–3752.
[33] T. Pauporte, J. Rathousky, *J. Phys. Chem. C* **2007**, *111*, 7639–7644.
[34] G. Wang, D. Chen, H. Zhang, J. Z. Zhang, J. Li, *J. Phys. Chem. C* **2008**, *112*, 8850–8855.
[35] J. H. Zeng, B. B. Jin, Y. F. Wang, *Chem. Phys. Lett.* **2009**, *472*, 90–95.
[36] Y. Wang, X. Li, G. Lu, X. Quan, G. Chen, *J. Phys. Chem. C* **2008**, *112*, 7332–7336.

Received: December 9, 2009
Revised: March 31, 2010
Published online: July 19, 2010

